1. Atomic and Molecular Science

1-1. Dynamics of Two Auger Electron Emission in Xe 4d Photoionization [1]

The creation of an inner-shell hole in an atom or molecule is usually followed by the emission of an Auger electron, a characteristic signature of both the hole and the species:

$$h\nu + M \rightarrow M^{+} + e^{-}_{\text{innershell photoelectron}}$$
$$\text{followed by} \qquad M^{+} \rightarrow M^{2+} + e^{-}_{\text{Auger}}.$$

When the photon energy is close to the threshold of the inner-shell hole creation, the subsequent Auger decay may be influenced by the photoelectron still existing in the vicinity of the M^{+} ion. The Auger peak becomes asymmetric and broadened, and its maximum is shifted to a higher energy. This so-called postcollsion interaction (PCI) is explained in terms of an interaction among the two outgoing electrons and the ion.

Our interest here goes to the much-less common, but richer, process where two Auger electrons are emitted. We chose to study the decay of the 4d hole in xenon atoms:

$$h\nu + Xe \rightarrow Xe^{+}(4d^{-1}) + e^{-}_{\text{4d photoelectron}}$$
$$\rightarrow \quad Xe^{3+} + e^{-}_{\text{4d photoelectron}} + e^{-}_{\text{Auger1}} + e^{-}_{\text{Auger2}}.$$

The two Auger electrons are emitted either simultaneously (double Auger: DA) or in sequence (cascade Auger: CA):

$$\text{DA: } Xe^{+}(4d^{-1}) \rightarrow Xe^{3+}\,{}^{4}S + e^{-}_{\text{Auger1}} + e^{-}_{\text{Auger2}},$$
$$\text{CA: } Xe^{+}(4d^{-1}) \rightarrow Xe^{2+} + e^{-}_{\text{Auger1}}$$
$$\rightarrow Xe^{3+}\,{}^{4}S + e^{-}_{\text{Auger1}} + e^{-}_{\text{Auger2}}.$$

It is a four-body dissociation as a whole process, in which one can expect a strong electron correlation. In order to gain insight into the dynamics of this decay, we detect the two Auger electrons

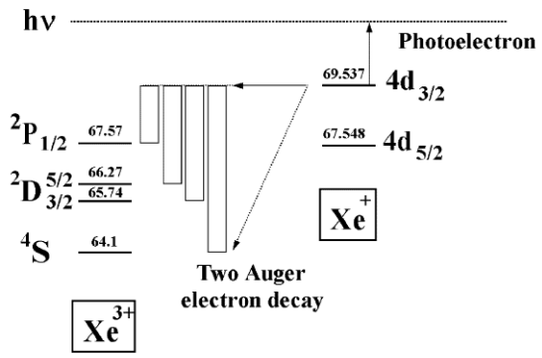

Figure 1.
Energy diagram of Xe^{+} and Xe^{3+} in the vicinity of Xe $4d^{-1}$ state.

in coincidence in the 4d photoionization threshold region where the PCI effect may be enhanced. Following the Xe energy level diagram in Fig. 1, the total energy of the two Auger electrons is 5.4 eV for the decay of the Xe^{+} of the $4d_{3/2}$ hole to the $Xe^{3+}\,{}^{4}S$ ground state. In our experimental setting, we have two electron energy analyzers: one is for threshold electrons with practically zero kinetic energy; the other is a hemispherical-type analyzer with a position-sensitive detector for energetic electrons. Figure 2 shows the electron spectrum measured at BL-16B with the hemispherical analyzer in coincidence with the threshold electron in the region where the photoelectron energy varies from near zero to 7.5 eV. All of the spectra reveal PCI effects that shift and broaden the line shapes, this distortion decreasing with increasing excess photon energy.

In the case of the DA process, the energy distribution of the two Auger electrons is continuous from 0 to 5.4 eV. However, the distribution will be discrete in the CA process depending on the energy levels of Xe^{2+}. Furthermore, two possibilities exist in the CA process: 1) the CA1 process, where an initial fast electron forms an intermediate state of the Xe^{2+*} ion, which decays to Xe^{3+} yielding a zero energy electron, and 2) the CA2 process, where the initial emission of a zero-energy electron forms Xe^{2+*} and its decay to Xe^{3+}, a fast electron. The theoretical

description of PCI distortion of the Auger lines is based on the eikonal approach for both the CA process and the DA process. We have calculated the incoherent contribution of the DA and CA1 processes (shown with broken blue line), and the CA2 process (shown with full red line) to the cross section, and estimated their role. Our calculations show a quite reasonable agreement of the CA2 curves with the experimental data compared to those for DA and CA1. The best agreement with the experiment was obtained for a width of the intermediate Xe^{2+*} state (Γ) in the range 45 meV < Γ < 70 meV. We have for the first time demonstrated from a comparison of the experimental data with the prediction in our calculations that the dominant process is cascade emission of a slow Auger electron followed by a rapid one, in both $4d_{5/2}$ and $4d_{3/2}$ decay, and the existence of intermediate Xe^{2+*} states very close to the Xe^{+} $4d_{5/2}$ and $4d_{3/2}$ states.

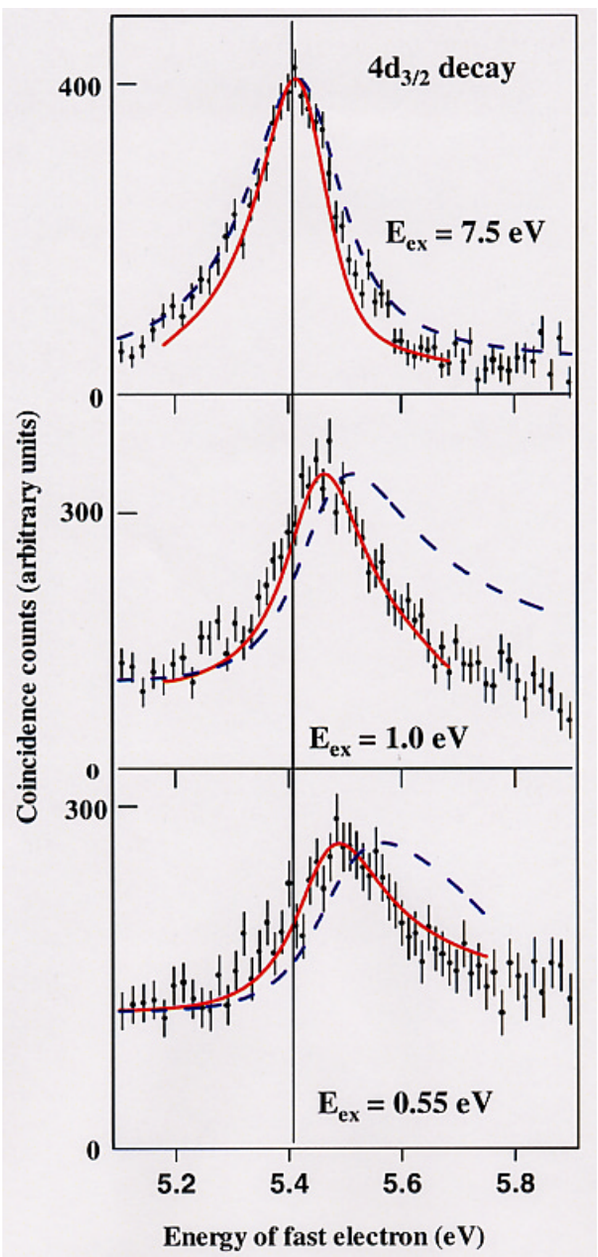

Figure 2.
Coincidence Spectra of a slow and a fast Auger electron in Xenon. The 5.4 eV peak selects the decay of the $4d_{3/2}$ hole to the Xe^{3+} ground state. Calculations: full red line is CA2 process, broken blue line is DA or CA1 process.

P. Lablanquie[1] and K. Ito[2] ([1]LURE, [2]KEK-PF)

References

[1] P. Lablanquie, S. Sheinerman, F. Penent, R.I. Hall, M. Ahmad, Y. Hikosaka and K. Ito, Phys. Rev. Lett., 87 (2001) 053001.

1-2. Rotationally Resolved PFI-ZEKE Spectra of the B $^2\Sigma_u^+$ (v^+=0) State of N_2^+

The pulsed-field ionization zero-kinetic-energy photoelectron (PFI-ZEKE) technique has made possible rotationally resolved spectroscopic studies of ions. These high-resolution studies have shown to provide valuable insight into the basic photoelectron dynamics of diatomic molecule. Most of the PFI-ZEKE studies were performed using lasers as the light source. Due to the difficulty of tuning lasers over a wide energy range, laser-based PFI-ZEKE studies generally cover only a few vibrational levels near a molecule's first ionization threshold. Hsu et al. [1] recently developed a new PFI-ZEKE detection scheme using multi-bunch synchrotron radiation. In their scheme, molecules are excited to high-n Rydberg states just below the ionization threshold using high-resolution monochromatized multi-bunch synchrotron radiation. A pulse electric field is then applied in the storage-ring dark gap to field-ionize

the Rydberg states. The electrons are collected with a steradiancy analyzer and a hemispherical energy analyzer. We used a penetrating field threshold electron analyzer instead of the steradiancy analyzer (Onuma et al. [2]) to eliminate any undesired hot electrons more efficiently. The rotationally resolved PFI-ZEKE spectra of the B $^2\Sigma_u^+$ (v^+=0) state of N_2^+ were first recorded at BL-20A using the PF synchrotron radiation dark gap [3]. Figure 3 shows in the upper part the ZEKE spectrum obtained at a resolution of 2.5 cm^{-1} and in the lower part a spectral simulation using the BOS model [4]. The transition from the X $^1\Sigma_g^+$ state to the B $^2\Sigma_u^+$ state involves a change in the rotational angular momentum by an odd quantum number, i.e., $\Delta J = \pm 1, \pm 3, \ldots$etc. It was found that this selection rule is valid for our observations. In Fig. 3, the P and R branches dominate and the N and T branches are weak. This result is supported by a previous study (Baltzer et al. [5]). However, the ZEKE spectrum is remarkably different from the simulated one in the low-energy side of the band origin. The enhancement of the L, N, and P branches can be attributed to field-induced rotational autoionization, like the autoionization mechanism of the Rydberg states converging to the N_2^+ X $^2\Sigma_g^+$ vibrational states.

The relative intensities (σ ($N^+ \leftarrow N''$)) for rotationally resolved structures in individual vibrational bands were simulated using the Buckingham-Orr-Sichel (BOS) model [4], which is described by the formula

$$\sigma (N^+ \leftarrow N'') \propto \Sigma_\lambda Q(\lambda; N^+, N'') C_\lambda ,$$

where N^+ and N" are the rotational quantum numbers of the ion and the neutral ground state, respectively.

This model was derived to predict the rotational line strengths σ ($N^+ \leftarrow N''$) observed in the single-photon ionization of diatomic molecules. The factor C_λ is associated with the electric transition moments, which is a linear combination of the electron transition amplitudes for the possible angular momenta (l) of the ejected electron. The other factor (Q) is determined by the angular-momentum coupling scheme. The parameter λ can be interpreted as the orbital angular-momentum quantum number of the electron partial waves before photoexcitation. Since the

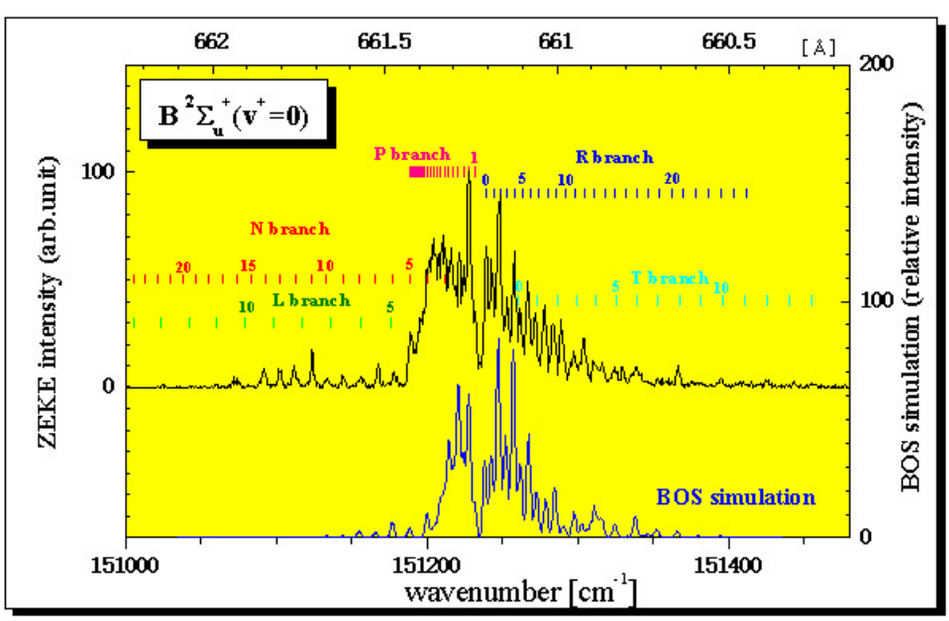

Figure 3.

(Black line) PFI-ZEKE photoelectron spectra of nitrogen (N_2^+B $^2\Sigma_u^+$(v^+=0) ← N_2X $^1\Sigma_g^+$(v''=0)) recorded with an extraction field of 0.8 V/cm between the dark gap of PF synchrotron. (Blue line) A simulation by the BOS model.

BOS model can be thought as a linear combination of spectra weighted by a set of the C_λ coefficients, these coefficients are determined by the measured spectrum least-squares fit. The ratio C_3/C_1 of the BOS coefficient obtained by the simulation was 0.35. Baltzer et al. [5] have obtained a branching ratio 0.18 for the T and R branches of the photoelectron spectrum of the B $^2\Sigma_u^+$ (v^+=0) band using the He I resonance line. If we converted the ratio C_3/C_1 to the branching ratio (T/R), the ratio was 0.17±0.02. This ratio agrees well with that of the Baltzer et al. study. This result suggests that relative ionization cross section can be evaluated if the effects due to the autoionization are negligibly small in the ZEKE spectrum.

Y. Morioka, H. Yoshii and T. Aoto (Tsukuba Univ.)

References

[1] C.-W. Hsu, M. Evans, P.A. Heimann and C.Y.Ng, Rev. Sci. Instrum. 68 (1997) 1694.

[2] T. Onuma, H. Yoshii, H. Ishijima, Y. Itou, T. Hayaishi and Y. Morioka, J. Mol. Spectrosc. 198 (1999) 209.

[3] T. Aoto, H. Yoshii and Y. Morioka, to be published in J. Chem. Phys.

[4] A.D. Buckingham, B.J. Orr and J.M. Sichel, Phil. Trans. Roy. Soc. London A 268 (1970) 147.

[5] P. Baltzer, L. Karlsson, and B. Wannberg, Phys. Rev. A 46 (1992) 315.

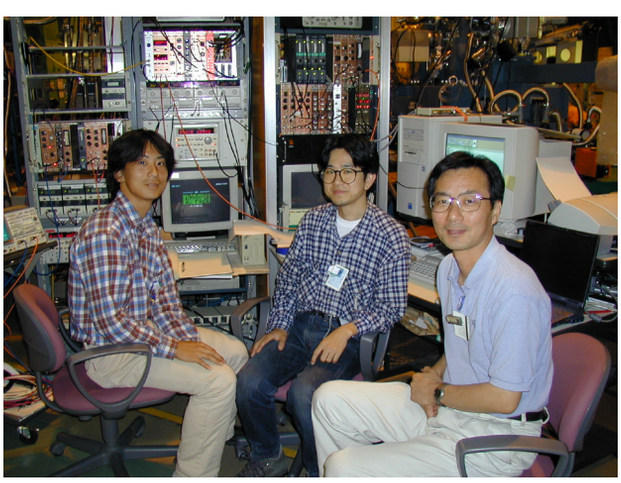

1-3. Effects of Light Polarizations on the $2\sigma_g$ Photoelectron Angular Distributions from Oriented N_2 Molecules

To perform a “complete” quantum-mechanical experiment, from which one can extract all of the-oretical parameters describing the process under consideration, is an ultimate goal of all photoionization experiments. One way to obtain the necessary parameters is to measure the photoelectron angular distributions (PAD) from oriented molecules under three different experimental configurations and one light polarization state. The other way is to measure PAD under one experimental configuration and three different light polarization states. Here, the latter approach towards the complete experiment is discussed.

Experimental results on PAD from the $2\sigma_g$ inner valence shell of N_2 molecules are shown in Fig. 4. The photons emitted from the helical undulator beamline of BL-28A were monochromatized and tuned at 58.2 eV. The molecular axis is aligned to the vertical line, and the polarization ellipse is indicated in the figure. As can be seen from the figure, PAD

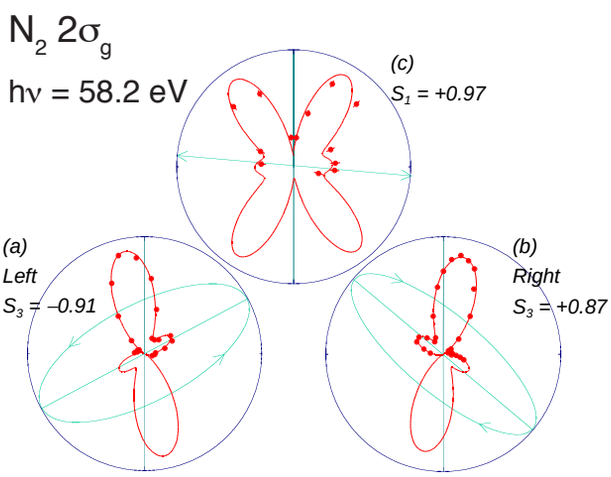

Figure 4.

$2\sigma_g$ photoelectron angular distributions for N_2 molecules oriented along the vertical line: (a) left-elliptical polarization, S_1 = 0.42 and S_3 = –0.91 (b) right-elliptical polarization, S_1 = 0.50 and S_3 = 0.87, (c) linear polarization, S_1 = 0.97 .

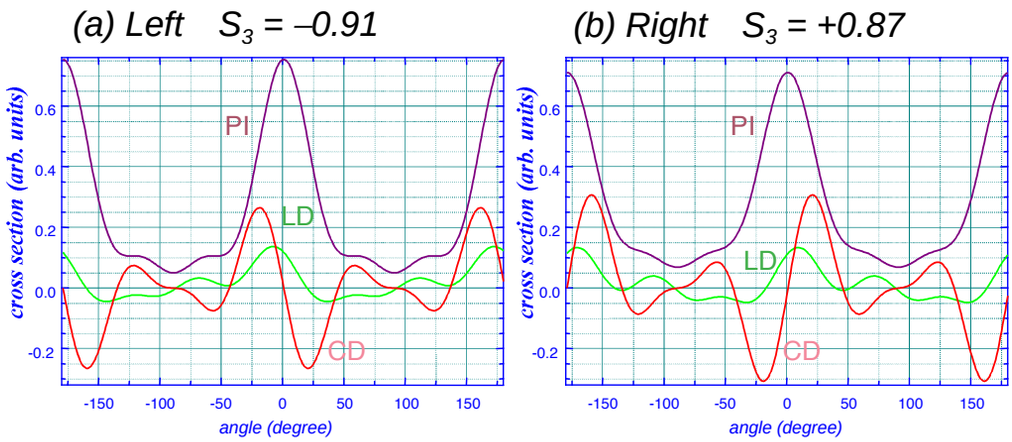

Figure 5.

Individual components of PAD: (a) left-elliptical polarization (b) right-elliptical polarization. The polarization properties are the same as in Fig. 4.

is strongly dependent on the light polarization. PAD can be written as the incoherent sum of four contributions, $d\sigma_t$ ($d\sigma_X$ and $d\sigma_Y$ refer to linearly polarized light with the electric vector along the x-axis and the y-axis, and $d\sigma_R$ and $d\sigma_L$ to right- and left-circularly polarized light):

$$d\sigma_{obs} = \frac{1}{2}(d\sigma_X + d\sigma_Y) + \frac{S_1}{2}(d\sigma_X - d\sigma_Y) + \frac{S_3}{2}(d\sigma_R - d\sigma_L) \quad , (1)$$

where S_1 and S_3 are the Stokes parameters describing the light polarization, and the individual $d\sigma_t$ includes the electric-dipole matrix elements and phase shifts describing the photoionization process and the angle between the molecular axis and the major axis of the polarization ellipse. The difference between Fig. 4(a) and Fig. 4(b) is caused by the opposite sign of S_3 and the major axes of the polarization ellipses being nearly orthogonal to each other. In other words, one can say that the difference is the mixture of, so-called, linear and circular dichroism. The circular dichroism already appears in the electric-dipole approximation, and arises solely from interferences between degenerate photoelectron continua with m values differing by ±1. Since the matrix elements and phase shifts have been determined by analyzing the experimental results of Fig. 4, every contribution, i.e., the first term (PI) independent on polarization of Equation (1), the second term (LD) dependent on S_1, and the third term (CD) dependent on S_3 are reconstructed as shown in Figure 5. The difference between the second terms in Figs. 5(a) and (b) gives the linear dichroism, and the difference between the third terms gives the circular dichroism. Because the circular dichroism in PAD appears in the electric-dipole approximation, as mentioned above, the magnitude of the circular dichroism is appreciably strong and of the same order of magnitude as the photoelectron intensity.

The interpretation of the PAD patterns for adsorbed molecules has been based on theoretical calculations for oriented free molecules. As discussed above, the theoretical parameters describing the photoionization process for free molecules can be determined experimentally. Using the determined parameters, one can simulate the PAD patterns for the relevant adsorbed molecules under the given geometrical condition and polarization properties. The difference between the simulated and experimental PAD patterns would be attributed to a surface effect, which is expected to be appreciable for chemisorbed molecules. The PAD measurements for free oriented molecules are quite useful for understanding the nature of the adsorbed molecules.

A. Yagishita (KEK-PF)